Contribution from the Chemistry Department,
York University, North York, Ontario, Canada M3J 1P3

Perchlorinated Phthalocyanines: Spectroscopic Properties and Surface Electrochemistry

M. Neal Golovin, Penny Seymour, Karupiah Jayaraj, YanSong Fu, and A. B. P. Lever*

Received August 15, 1989

The electronic spectroscopic data for zinc, cobalt, and iron perchlorinated phthalocyanines in several oxidation states are discussed. The magnetic properties of the iron(II) and cobalt(II) derivatives from ambient temperature to 5 K are reported. The electrochemical behavior of these three species is reported in solution and as surfaces on highly oriented pyrolytic graphite. The pH dependence of the surface data is analyzed in detail. The first clearly defined reduction process corresponds with $M^{I}[Cl_{16}Pc(-2)]^{-}/M^{I}[Cl_{16}Pc(-3)]^{2-}$ for M = Co and Fe. The iron and cobalt species' $M^{II}Pc(-2)/[M^{I}Pc(-2)]^{-}$ redox process are broad or ill-defined on the surface and absent from solution. The $Fe^{III}[Cl_{16}Pc(-2)]^{+}/Fe^{II}[Cl_{16}Pc(-2)]$ redox process has atypical pH dependence. The data are explained in terms of the acceptor nature of the chlorine substitution. Oxygen reduction data, catalyzed by these species, are also reported.

Introduction

Perchlorinated phthalocyanine derivatives have been reported in the literature,[1,2] but their chemical and physical properties have not been investigated in any depth. We report here our results on the preparation and spectroscopic and electrochemical (surface and solution) properties of the iron, cobalt, and zinc derivatives, $M[Cl_{16}Pc(-2)]$.

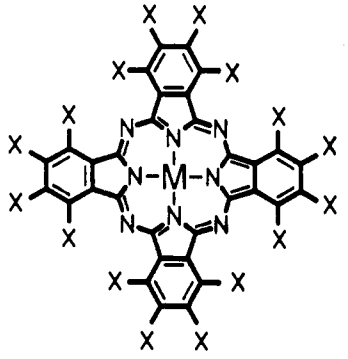

X = H MPc

X = Cl M = Fe 1

X = Cl M = Zn 2

X = Cl M = Co 3

The electrocatalysis of the cathodic reduction of O_2 at $M[Cl_{16}Pc(-2)]$-modified graphite electrodes has also been studied here. The electron acceptor character of the substituents imposes some well-defined changes on the properties of these complexes relative to unsubstituted or electron donor substituted species. These perchlorinated species are under intense study industrially as optical recording medium substrates, infrared light detectors, reprographic photoreceptors, etc., as witnessed by the existence of many patents.[3-12]

Experimental Section

The solvents used in the syntheses, namely, acetone, methylene chloride, and *N*,*N*-dimethyl formamide (DMF), were all reagent grade and were used as supplied.

The complexes were prepared by a template reaction[1,2] involving the reaction of tetrachlorophthalic anhydride, urea, ammonium molybdate, and the appropriate metal salt ($FeCl_2 \cdot 4H_2O$ for $Fe[Cl_{16}Pc(-2)]$ (**1**) and $Zn(C_2H_3O_2) \cdot 2H_2O$ for $Zn[Cl_{16}Pc(-2)]$ (**2**)), heated in nitrobenzene to 200 °C for 4-8 h. After cooling, the solutions were diluted with ethanol, boiled for 10 min, and filtered hot. These products were purified further by refluxing in 1% aqueous HCl and then 1% aqueous NaOH. The filtered products were then dissolved in concentrated H_2SO_4, the solutions filtered, and the products recovered by pouring this filtrate over ice. The zinc product was further purified by recrystallization from DMF. The iron product was further purified by extraction with methylene chloride and acetone (the pure product remaining in the Soxhlet thimble). Both products analyzed satisfactorily (Anal. C, N).

The cobalt complex, $Co[Cl_{16}Pc(-2)]$ (**3**), was prepared in a similar manner by using $CoCl_2 \cdot 4H_2O$ and tetrachlorophthalonitrile instead of the anhydride and urea. After the final extraction with methylene chloride, the cobalt derivative was purified by extraction with DMF, leading to dissolution and recovery of a DMF mono adduct. (Anal. C, H, N).

Magnetic Data. Data were collected by using the Faraday method and equipment previously described.[13] We are indebted to Prof. L. K. Thompson, Memorial University, for the collection of these data. All data are presented in the format temperature in Kelvin, molar susceptibility in centimeters cubed per mole in scientific notation, magnetic moment in Bohr magnetons.

$Fe[Cl_{16}Pc(-2)]$ (mol wt = 1119.4, diamagnetic correction 617×10^{-6} cm^3 mol^{-1}): 5.41, 1.059E-01, 2.140; 7.93, 9.650E-02, 2.474; 12.65, 7.771E-02, 2.804; 17.35, 6.361E-02, 2.971; 22.11, 5.307E-02, 3.063; 27.10, 4.469E-02, 3.112; 32.21, 3.825E-02, 3.139; 36.95, 3.357E-02, 3.150; 41.65, 2.986E-02, 3.154; 45.35, 2.755E-02, 3.161; 49.51, 2.502E-02, 3.148; 54.28, 2.292E-02, 3.154; 59.26, 2.104E-02, 3.158; 64.54, 1.929E-02, 3.155; 70.08, 1.784E-02, 3.162; 75.21, 1.662E-02, 3.161; 80.17, 1.557E-02, 3.160; 84.68, 1.467E-02, 3.152; 92.91, 1.336E-02, 3.151; 103.22, 1.204E-02, 3.153; 113.95, 1.093E-02, 3.156; 125.00, 1.005E-02, 3.169; 135.20, 9.319E-03, 3.174; 145.27, 8.709E-03, 3.181; 164.53, 7.743E-03, 3.192; 184.33, 6.929E-03, 3.196; 204.69, 6.299E-03, 3.211; 225.21, 5.776E-03, 3.225; 246.68, 5.348E-03, 3.248; 261.61, 4.983E-03, 3.229; 281.29, 4.681E-03, 3.245; 297.53, 4.491E-03, 3.269.

$Co[Cl_{16}Pc(-2)]$ (mol wt = 1123, diamagnetic correction 617×10^{-6} cm^3 mol^{-1}): 5.27, 6.864E-03, 0.538; 7.57, 5.423E-03, 0.573; 12.48, 4.173E-03, 0.645; 17.18, 3.687E-03, 0.712; 21.93, 3.416E-03, 0.774; 26.95, 3.236E-03, 0.835; 32.08, 3.125E-03, 0.895; 36.81, 3.050E-03, 0.948; 41.61, 3.000E-03, 0.999; 45.23, 2.980E-03, 1.038; 49.39, 2.983E-03, 1.085; 54.10, 3.010E-03, 1.141; 59.07, 3.009E-03, 1.192; 64.34, 2.959E-03, 1.234; 69.49, 2.907E-03, 1.271; 74.52, 2.871E-03, 1.308; 79.49, 2.847E-03, 1.345; 84.10, 2.825E-03, 1.378; 92.64, 2.789E-03, 1.438; 103.38, 2.745E-03, 1.506; 113.56, 2.697E-03, 1.565; 124.59, 2.649E-03, 1.625; 134.68, 2.597E-03, 1.673; 144.68, 2.550E-03, 1.718; 163.94, 2.451E-03, 1.793; 183.62, 2.344E-03, 1.855; 203.83, 2.256E-03, 1.918; 224.47, 2.172E-03, 1.974; 245.48, 2.089E-03, 2.025; 264.22, 2.019E-03, 2.065; 280.33, 1.957E-03, 2.095; 296.47, 1.917E-03, 2.132.

FTIR Data (Nujol mulls, cm^{-1}): **1**, 721 m, 753 m, 772 s, 780 sh, 956 s, 1100 m, 1158 vs, 1214 vs, 1274 s, 1308 vs, 1313 m; **2**, 722 w, 747 s,

(1) Birchall, J. M.; Haszeldine, R. N.; Morley, J. O. *J. Chem. Soc. C* **1970**, 2667-72.
(2) Metz, J.; Schneider, O.; Hanack, M. *Inorg. Chem.* **1984**, *23*, 1065-71.
(3) Yoshiike, N.; Kondo, S. Japan Patent JP 86/211849, 1986.
(4) Takume, H.; Kuroda, S.; Alga, H. Japan Patent 86/308915, 1988.
(5) Kuroiwa, A.; Nanba, N.; Kamijo, T. Japan Patent 86/24609, 1986.
(6) Suzuki, T.; Murayama, T.; Ono, H.; Otsuka, S.; Nozomi, M. European Patent EP 180931, 1986.
(7) Duggan, P.; Gordon, P. F. European Patent EP 155780, 1985.
(8) Ricoh Co. Ltd. Japan Patent JP 88/60796, 1988.
(9) Hung, Y.; Klosse, T. R.; Regan, M. T.; Rossi, L. J. U.S. Patent 4701396, 1987.
(10) Sato, T. Japan Patent 86/162385, 1986.
(11) Ricoh Co. Ltd. Japan Patent JP 83/56892, 1983.
(12) Ricoh Co. Ltd. Japan Patent JP 83/112794, 1983.
(13) Mandal, S. K.; Thompson, L. K.; Gabe, E. J.; Lee, F. L.; Charland, J.-P. *Inorg. Chem.* **1987**, *26*, 2384-89.

0020-1669/90/1329-1719$02.50/0

771 s, 779 m, 941 vs, 1099 m, 1142 vs, 1207 s, 1274 m, 1302 s, 1320 m, 1326 m; **3**, 722 m, 752 m, 772 m, 780 w, 957 m, 1096 s, 1160 s, 1215 vs, 1275 s, 1305 m, 1315 m.

Solutions for spectroscopy, electrochemistry, and spectroelectrochemistry were prepared in DMF (Aldrich, Gold Label). Solutions for spectroelectrochemistry, cyclic voltammetry, and differential-pulse polarography contained 0.1 M LiCl (recrystallized from water and dried under vacuum) as supporting electrolyte and were maintained under nitrogen. Spectra were recorded in DMF that had been deoxygenated either by bubbling with nitrogen or by several freeze–pump–thaw cycles.

Buffer solutions were prepared from 0.1 M solutions of reagent grade H_3PO_4, KH_2PO_4, K_2HPO_4, and KOH and adjusted to the desired pH and to an approximately constant ionic strength. Distilled water for buffer solutions was double distilled in glass from alkaline $KMnO_4$ and then passed through a Barnstead organic removal cartridge and two Barnstead mixed-resin ultrapure cartridges. Argon, nitrogen, and oxygen were used as supplied. Buffer solutions were saturated with argon or oxygen for about 1 h and maintained under an atmosphere of the appropriate gas during data collection. Oxygenated solutions contained an oxygen concentration of approximately 10^{-3} M.

Electronic spectra were recorded with a Hitachi-Perkin-Elmer Model 340 microprocessor-controlled spectrometer or a Guided Wave Inc. Model 100-20 optical waveguide spectrum analyzer. Spectroelectrochemical data were recorded as for spectra by using a PAR Model 173 potentiostat with a two-compartment cell. A platinum-junction SCE, separated from the working electrode with a Luggin capillary for contact, served as a reference. A platinum basket was employed as the working electrode, and the auxiliary electrode was a platinum wire separated from the bulk of the solution by a ceramic frit. Spectra were recorded during bulk electrolysis by immersing the fiber optic probe in the solution[14] or by using a cell with inset windows for use with a conventional spectrometer.

Modified HOPG electrodes were prepared as previously described,[15,16] and the catalyst was adsorbed for about 30 min (minimum time to ensure equilibrium adsorption) from solutions of $(0.5–1) \times 10^{-4}$ M in DMF.

Results and Discussion

Electronic and Geometric Structure. (i) Magnetism. The iron complex **1** is a typical iron(II) square-planar phthalocyanine with no axial coordination. Its room-temperature magnetic moment is 3.27 μ_B compared with 3.85 μ_B for unsubstituted FePc[17–19] and attributable to intermediate spin $S = 1$.

The magnetic properties follow the Curie–Weiss law with an apparent Curie–Weiss constant of −4.9 K (see Experimental Section). However, as shown in Figure 1, there is a sharp reduction in magnetic moment occurring below about 25 K, falling to 2.14 μ_B at 5 K. This behavior is remarkably similar to that of unsubstituted FePc except that, in this latter case, the sharp reduction in magnetic moment begins at about 60 K.[18]

The magnetic properties of FePc are well described in terms of a $^3B_{2g}$ ground term with zero-field splitting, D, of the $M_s = 0$ (lowest) and $M_s = \pm 1$ magnetic spin components. The relevant parameters are $g_\parallel = g_\perp = 2.74$ and $D = 64$ cm^{-1}.[18]

If exactly the same model is used to explain the magnetic data for species **1**, then an adequate fit of the average magnetic moment can be obtained with the parameters $g_\parallel = 2.22$, $g_\perp = 2.28$, $D = 16$ cm^{-1} and TIP $= 140 \times 10^{-6}$ cm^3 mol^{-1} (Figure 1). A detailed single-crystal anisotropy study is necessary to prove the validity of this data set, since the fit is not unique. Within this model, the sharp decrease in magnetic moment near 20 K does require D to lie in the range 17 ± 5 cm^{-1}, while the fit at higher temperatures requires the average g value to be close to 2.26 ± 0.05; however, the individual g values may deviate from the values quoted here. The lower moment, of **1** relative to FePc, can be explained in terms of changes in the coupling of ground- to excited-state terms (variation in g factor) rather than in an exchange-coupling mechanism, which does not need to be introduced.

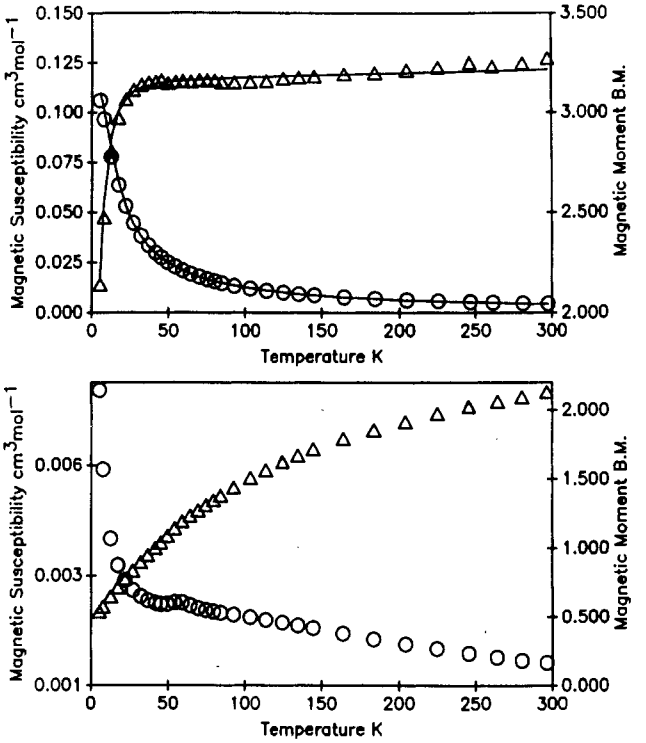

Figure 1. Magnetic data for (top) iron (**1**) and (bottom) cobalt (**3**) species. The open triangles show the magnetic moment data and are referenced to the right-hand y axis, while the open circles illustrate the magnetic susceptibility and are referenced to the left-hand axis. The solid lines through the iron data are those calculated on the basis of the model of the $^3B_{2g}$ ground term split by the zero field. See text for details and parameters.

The cobalt complex **3** exhibits a room temperature magnetic moment of 2.13 μ_B compared with 2.72 μ_B for CoPc[17,20,21] and associated with an $S = {}^1/_2$ intermediate spin square-planar cobalt(II) phthalocyanine. However the temperature dependence is unusual. Down to about 50 K, the susceptibility follows the Curie–Weiss law but with an apparent Curie–Weiss constant of −350 K (Figure 1). Below 50 K the susceptibility increases rapidly, indicating a change in the coupling process has occurred.

Unsubstituted CoPc shows only a relatively small change in magnetic moment between room temperature and 80 K and fits a simple model involving a d_{z^2} ground state.[20,21] This model is quite unable to explain the behavior of the cobalt species, **3**. It is likely that there is an exchange process occurring in this system, but single-crystal anisotropy studies are needed to unravel this distinctive behavior.

(ii) Solubility. These three complexes have exceedingly low solubilities in essentially all solvents, which leads to considerable difficulty in obtaining reliable data therefrom. Sonication in solvents such as DMF or DMSO leads to a moderately strongly colored solution, but such "solutions" generally dropped some sediment upon standing—it is likely that they are not true solutions. The addition of electrolyte (e.g., tetrabutylammonium hexafluorophosphate ((TBA)PF_6) and tetrabutylammonium perchlorate (TBAP)) to DMF "solutions" prompted the complexes to precipitate, causing difficulty in obtaining solution electrochemical data of high quality. Indeed on standing overnight, such solutions became colorless.

The addition of chloride ion does lead to slightly greater solubility, via complexation, especially for the oxidized species. The addition of hydrazine causes greater solubility of the iron and zinc complexes, also because of complexation, but causes reduction of the cobalt complex.

(14) Nevin, W. A.; Wei, L. *Anal. Sci.* **1988**, *4*, 559–63.
(15) Janda, P.; Kobayashi, N.; Auburn, P. R.; Lam, H.; Leznoff, C. C.; Lever, A. B. P. *Can. J. Chem.* **1988**, *67*, 1109–19.
(16) Hempstead, M. R.; Lever, A. B. P.; Leznoff, C. C. *Can. J. Chem.* **1987**, *65*, 2677.
(17) Lever, A. B. P. *J. Chem. Soc.* **1965**, 1821–29.
(18) Barraclough, C. G.; Martin, R. L.; Mitra, S.; Sherwood, R. C. *J. Chem. Phys.* **1970**, *53*, 1643–48.
(19) Dale, B. W.; Williams, R. J. P.; Johnson, C. E.; Throp, T. L. *J. Chem. Phys.* **1968**, *49*, 3441.
(20) Martin, R. L.; Mitra, S. *Chem. Phys. Lett.* **1969**, *3*, 183–4.
(21) Gregson, A. K.; Martin, R. L.; Mitra, S. *J. Chem. Soc., Dalton Trans.* **1976**, 1458–66.

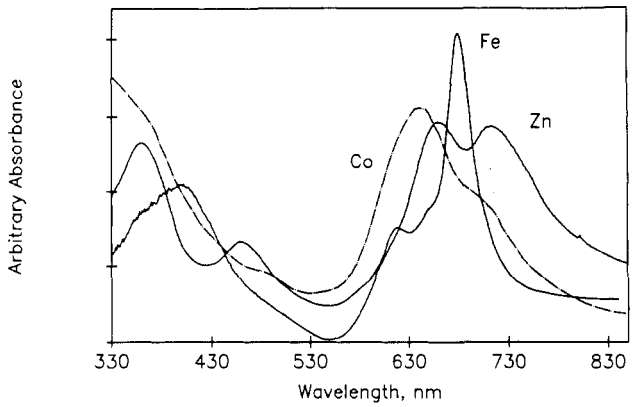

Figure 2. Electronic spectroscopic data for species **1–3** "dissolved" in argon-purged DMF.

Because of these problems spectroelectrochemical studies, with one exception, did not yield isosbestic points, as is commonly expected in such experiments,[22,23] and molar extinction coefficients are not reliably obtained.

Nevertheless, it is possible to obtain definitive characterization data for these species in order to investigate the effect of 16 chlorine substituents upon their chemistry.

(iii) Electronic Spectra. (a) Organic Solvent Data. Complexes **1–3**, when freshly "dissolved" in nitrogen-purged DMF, yield the electronic spectra shown in Figure 2. The cobalt and zinc species spectra are typical of aggregated phthalocyanine with dilution having little effect upon the spectrum. The iron complex, **1**, spectrum, is that of a largely nonaggregated iron(II) phthalocyanine.[15,24] The presence of the charge-transfer band in the region 400–500 nm is typical of an axially coordinated iron(II) phthalocyanine.[24-27] There is some variability in these spectra from one sample to the next.

If **1** is "dissolved" in aerated DMF, or the nitrogen-purged solution is allowed to absorb oxygen, or faster if the solution is heated in the presence of oxygen, the Q band broadens and shifts toward the blue region (Table I). Upon reduction of this oxidized solution, the higher energy component of the Q band diminishes first in intensity relative to the lower energy component; there is no similar change in intensity when the species is oxidized. It is most likely that **1** forms a μ-oxo dimeric species $[Cl_{16}Pc(-2)]Fe^{III}-O-Fe^{III}[Pc(-2)Cl_{16}]$ (**4**) when "dissolved" in aerated DMF—such species typically absorb strongly near 620 nm.[28-31] This species, **4**, reverts to **1** when heated in degassed DMF. It was not isolated.

The redox species accessible to these various complexes were determined by spectroelectrochemical studies. When reduced in DMF/LiCl at −0.80 V vs SCE, species **1** yields a spectrum typical of $[Fe^{I}Pc]^-$ (Table I).[32,33] Reoxidation at 0.00 V regenerates the $Fe^{II}Pc$ spectrum (Table I). Solubility problems and the absence of isosbestic points prevent an analysis during the Nernst equation to determine the precise position of the Fe(II)/Fe(I) couple. However, the $Fe^{II}[Cl_{16}Pc(-2)]/Fe^{I}[Cl_{16}Pc(-2)]^-$ couple must lie between 0.00 and −0.80 V vs SCE under these conditions.

When **1** is oxidized at 0.65 V vs SCE, the characteristic $Fe^{II}Pc$ charge-transfer band observed near 500 nm for species **1** in DMF/LiCl diminished in intensity relative to the Q band but a completely oxidized $Fe^{III}Pc$ species was not obtainable below the solvent oxidation limit. Thus, the $Fe^{III}[Cl_{16}Pc(-2)]^+/Fe^{II}[Cl_{16}Pc(-2)]$ solution oxidation potential for species **1** is near and possibly slightly above 0.65 V in DMF/LiCl.

Reduction of the zinc species, **2**, in DMF/LiCl did yield isosbestic points (Figure 3) showing reduction to $Zn^{II}[cl_{16}Pc(-3)]^-$ (**5**) in a clean process where the reduced species could be reoxidized to starting species **2**. An analysis using the Nernst equation yielded

Table I. Electronic Spectral Data[a] (λ_{max}, nm)

Complex	Note	Electronic spectra (nm)	Ref.
Fe(II)[Cl_{16}Pc(-2)]	(b)	361s 460 619 678s	tw
	(c)	345 641s 682sh	tw
	(d,e)	352 382 469 623 685s	tw
Fe(II)Pc(-2)	Py	324s 410m 654s	15
Fe(I)[Cl_{16}Pc(-2)]$^-$	DMF/LiCl	400br 537s 654w 687m 805m	tw
[(Py)Fe(I)Pc(-2)]$^-$	Py/LiCl	324s 512vs 596m 661m 803m	32
[Fe(I)Pc(-2)]$^-$	THF	326vs 515vs 596w 665m 800m	33
Co(II)[Cl_{16}Pc(-2)]	(b)	316s 360sh 490sh 641s 706sh	tw
Co(II)TNPc(-2)	DCB	330s 380m 612m 645sh 678vs	23
Co(I)[Cl_{16}Pc(-2)]$^-$	(d)	326s 480vs 545sh 656s 701s	tw
[Co(I)Pc(-2)]$^-$	THF	312vs 467s 633m 694s	33
[Co(I)TNPc(-2)]$^-$	DCB	313vs 471s 520sh 600sh 643m 675sh 708s	23
Zn[Cl_{16}Pc(-2)]	(b)	378s 404sh 660s 711s	tw
	(d,e)	362 404 649 688	tw
ZnTNPc(-2)	DCB	356vs 614m 680vvs	22
Zn[Cl_{16}Pc(-3)]$^-$	DMF/LiCl	415m 474m 600m 625sh 698m 830sh	tw
		860sh 894m 928m	tw
[ZnPc(-3)]$^-$	THF	323s 562s 636s 948m	33
Zn[Cl_{16}Pc(-4)]$^{2-}$	DMF/LiCl	363br 553s 696mbr 842m	tw

[a] Absorption bands for a specific metal and oxidation state believed to have a common assignment are lined up together. [b] Argon-purged DMF. [c] Aerated DMF—this is likely a solution of $[Cl_{16}Pc(-2)]Fe^{III}-O-Fe^{III}[Cl_{16}Pc(-2)]$. [d] Argon-purged DMF plus hydrazine. [e] These species likely contain axially coordinated hydrazine.

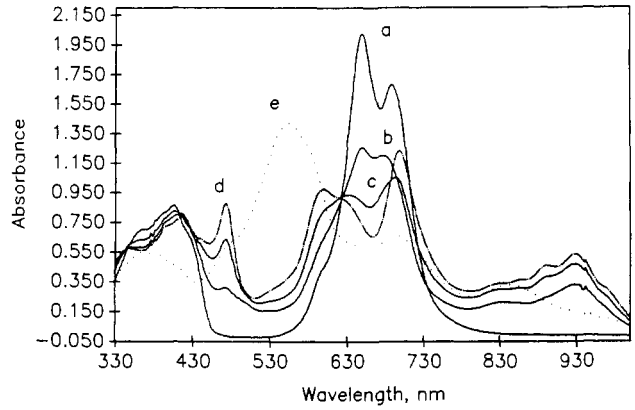

Figure 3. Spectroelectrochemical data for the reduction of zinc species **2** in DMF containing 0.1 M LiCl. The successive spectra are obtained with the platinum working electrode polarized at 0.0 (a), −0.6 (b), −0.7 (c), −0.8 (d), and −1.3 V (e). Spectrum a corresponds with the starting material **2**. Spectrum d is dominantly that of the anion radical **5** with a small contribution from that of the dianion radical **6**. Spectrum e is that of the dianion radical **6**.

(22) Manivannan, V.; Nevin, W. A.; Leznoff, C. C.; Lever, A. B. P. *J. Coord. Chem.* **1988**, *19*, 139–58.
(23) Nevin, W. A.; Hempstead, M. R.; Leznoff, C. C.; Lever, A. B. P. *Inorg. Chem.* **1987**, *26*, 570–77.
(24) Nevin, W. A.; Liu, W.; Melnik, M.; Lever, A. B. P. *J. Electroanal. Chem. Interfacial Electrochem.* **1986**, *213*, 217–34.
(25) Stillman, M. J.; Thompson, A. J. *J. Chem. Soc., Faraday Trans. 2* **1974**, *70*, 790.
(26) Dale, B. W. *Trans. Faraday Soc.* **1969**, *65*, 331.
(27) Kobayashi, N.; Nishigama, Y. *J. Phys. Chem.* **1985**, *89*, 1167.
(28) Ercolani, C.; Gardini, M.; Murray, K. S.; Pennesi, G.; Rossi, G. *Inorg. Chem.* **1987**, *25*, 3927.
(29) Ercolani, C.; Rossi, G.; Montanelli, F. *Inorg. Chim. Acta* **1980**, *44*, L215.
(30) Ercolani, C.; Gardini, M.; Pennesi, G.; Rossi, G. *Inorg. Chem.* **1983**, *22*, 2534.
(31) Lever, A. B. P.; Licoccia, S.; Ramaswamy, B. S. *Inorg. Chim. Acta* **1982**, *64*, L87.
(32) Lever, A. B. P.; Wilshire, J. P. *Inorg. Chem.* **1978**, *17*, 1145–51.
(33) Clack, D. W.; Yandle, J. R. *Inorg. Chem.* **1972**, *11*, 1738.
(34) Myers, J. F.; Rayner-Canham, G. W.; Lever, A. B. P. *Inorg. Chem.* **1975**, *14*, 461–8.

a redox potential of −0.60 V vs SCE for the $Zn^{II}[Cl_{16}Pc(-2)]/Zn^{II}[Cl_{16}Pc(-3)]^-$ redox process. Figure 3 also shows data for further reduction to the presumed $Zn^{II}[Cl_{16}Pc(-4)]^{2-}$ species (**6**). The isosbestic points are lost in this second reduction, but reoxidation does regenerate species **2**.

The spectrum of complex **3** (Figure 2) is dominated by aggregation, indicated by the very broad Q band[27,35,36] with a blue-shifted component near 640 nm.

Addition of hydrazine, or NaSH, to a DMF solution of complex **3** yields a spectrum typical of a $Co^{I}Pc$ species (Table I).[24,25,33,36] The same species is obtained by electrochemical reduction of a solution of **3** in DMF/LiCl at −0.8 V vs SCE. Reoxidation at 0.0 V yields a spectrum with a double Q band similar to that initially observed (Figure 2). The $Co^{II}[Cl_{16}Pc(-2)]/Co^{I}[Cl_{16}Pc(-2)]^-$ couple must lie between 0.00 and −0.80 V vs SCE in DMF/LiCl.

Oxidation of **3** in DMF/LiCl at 0.9 V yields a spectrum in which the Q band, centered at 690 nm, is relatively stronger and sharper; most of the higher energy Q component, observed in the spectrum of the cobalt(II) species, disappears, but there is no growth of absorption near 450–550 nm. This behavior is typical of the formation of a $Co^{III}[Cl_{16}Pc(-2)]^+$ species, which, however, could not be produced fully before the solvent oxidation limit.

Table I shows the data for these species in various oxidation states and data from the literature for unsubstituted or tetraneopentoxy-substituted phthalocyanines. In general there is close agreement between the relevant sets of data, providing further support for the oxidation state conclusions reached here. An apparent exception is the $Zn^{II}[Cl_{16}Pc(-3)]^-$ (**5**) anion radical, whose electronic spectrum appears rather different from that previously described for the unsubstituted $Zn^{II}Pc(-3)$ anion radical (**7**).[33] However closer examination shows significant similarity. Species **7** shows three absorption features between 25 000 and 15 000 cm^{-1}, one being a well-defined shoulder on the Soret region absorption. A fourth transition is evident as an ill-defined shoulder on the upper energy Q-band component.[37] In the spectrum of anion radical **5**, the shoulder on the Soret is red-shifted and now appears as a well-defined, narrow peak, while the upper energy component of the Q-band absorption is now clearly two absorptions.

There is a general trend that, with few exceptions, any given band (Q band, Soret, or charge transfer) in the spectrum of a $M[Cl_{16}Pc(-2)]$ species is shifted slightly to lower energy relative to the corresponding transition in the spectra of the other derivatives cited.

(b) Concentrated Sulfuric Acid Data. The three complexes dissolve in concentrated sulfuric acid without decomposition; their spectra are listed in Table II, along with the corresponding data for various other substituted and unsubstituted MPc derivatives. The striking aspect of the data is the very significant red shift in the position of the Q band. The position of the Q band in the sulfuric acid spectrum should be a measure of the basicity of the uncoordinated bridging nitrogen atoms in the macrocycle.[38,39] It is influenced critically by the nature and position of the phthalocyanine peripheral substituents.

If the data in Table II are compared, however, there is no simple relationship between substituent donicity and Q-band wavelength maximum. For example, within the group of copper phthalocyanines, electron donor substituents are seen to shift the maxima both to higher and lower wavelength relative to those of the unsubstituted species. In general, halogen substituents shift the Q-band maximum to longer wavelengths relative to the unsubstituted species, with chloride substitution being more effective than fluoride substitution in this respect. The observed shift probably involves a subtle interplay of the inductive and mesomeric properties of the substituent and its location on the peripheral benzene ring.

Table II. Spectroscopic Data for MX_nPc in Concentrated Sulfuric Acid: Position of the Q Band

M	X[a]	n[b]	Q-band max, nm[c]	ref
CoPc	Cl	16	832	tw
CoPc	4-O-*i*-Pr	4	815	tw
CoPc	H	16	786	tw
CoPc	4-CO_2H	4	756	tw
CoPc	3-NH_2	4	738	59
CoPc	3-NO_2	4	715	tw
ZnPc	Cl	16	868	tw, 1
ZnPc	4-O-NP[d]	4	829	tw
ZnPc	4-OBu	4	827	38
ZnPc	F	16	820	1
ZnPc	H	16	783	38
ZnPc	CN	8	756	38
ZnPc	4-NH_2	4	742	59
FePc	Cl	16	854	tw
FePc	H	16	785	tw
FePc	4-SO_3H	4	770	tw
CuPc	F	16	821	1
CuPc	4-*t*-Bu	4	808	43
CuPc	4-Cl	4	803	43
CuPc	H	16	791	43
CuPc	4-Me	4	786	43
CuPc	4-CO_2H	4	780	43
CuPc	4-NO_2	4	776	43
CuPc	4-SO_3H	4	771	43
CuPc	CN	8	728	39
CuPc	3-NO_2	4	728	43
CuPc	3-CO_2H	4	722	43
CuPc	4-PhO	4	838	39
CuPc	4-NH_2	4	749	59
VOPc	4-Bu	4	834	60
VOPc	Cl	16	862	60

[a] Substituent. [b] Number of substituents. [c] Maximum wavelength component. [d] NP = neopentoxy.

With use of Forster theory,[40,41] a red shift in the Q-band absorption would signify that the excited state was a stronger base than the ground state. Thus perchlorination has a substantial effect in increasing the basicity of the excited state relative to the ground state. Chloride substitution is expected to stabilize both the π and π^* states of the phthalocyanine ring.[42] The HOMO a_{2u} orbital has nodes at the peripheral nitrogen atoms, while the LUMO e_g orbital does have electron density at these positions.[42] Thus, protonation of any phthalocyanine will red-shift the $\pi-\pi^*$ transition relative to the unprotonated species, as is indeed evident.[43] To understand the reasons for the extraordinary red shifts seen with these species requires further experiment.

(iv) Fourier Transform Infrared Spectroscopy. All three species have very similar FTIR spectra (see Experimental Section), suggesting a similar crystal structure, though the data for iron and cobalt are more closely similar compared to the data for zinc.

(v) Electrochemistry. Electrochemical studies of **1–3** were carried out both with the complexes in solution and on a surface as a modifier on a highly oriented pyrolytic graphite (HOPG) electrode.

The surface electrochemistry was generally reproducible, though the first scan of a $M[Cl_{16}Pc(-2)]$-modified electrode was somewhat different from all subsequent scans. If the complexes are being deposited in an aggregated form, the adsorbed molecules may rearrange on the surface during the initial scanning process. Moreover, many of the redox waves seen in the study of these species were structured with shoulders, suggesting that there were several slightly different sites on the HOPG surface. All the waves

(35) Nevin, W. A.; Wei, L.; Lever, A. B. P. *Can. J. Chem.* **1987**, *65*, 855–58.
(36) Nevin, W. A.; Hempstead, R. H.; Wei, L.; Leznoff, C. C.; Lever, A. B. P. *Inorg. Chem.* **1987**, *26*, 570–77.
(37) Minor, P. C.; Gouterman, M.; Lever, A. B. P. *Inorg. Chem.* **1985**, *24*, 1894–1900.
(38) Wohrle, D.; Schmidt, V. *J. Chem. Soc., Dalton Trans.* **1988**, 549–51.
(39) Wohrle, D.; Schulte, B. *Makromol. Chem.* **1988**, *189*, 1167–87.
(40) Forster, T. *Naturwissenschaften* **1949**, *36*, 186.
(41) Weller, A. *Prog. React. Kinet.* **1961**, *1*, 189–214.
(42) Hale, P. D.; Pietro, W. J.; Ratner, M. A.; Ellis, D. E.; Marks, T. J. *J. Am. Chem. Soc.* **1987**, *109*, 5943–47.
(43) Gaspard, S.; Verdaguer, M.; Viovy, R. *J. Chem. Res., Synop.* **1979**, 271–74.

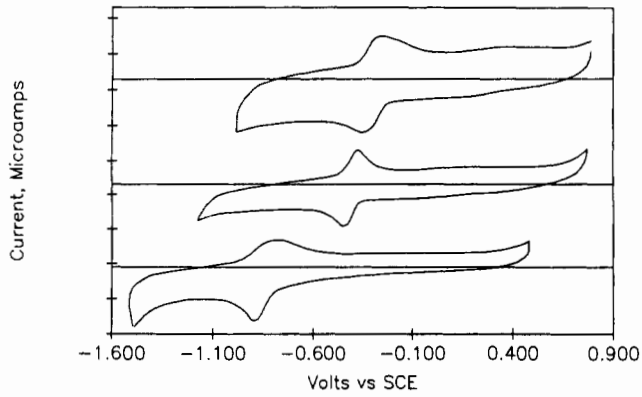

Figure 4. Surface electrochemical cyclic voltammograms for zinc species **2** under argon at (bottom) pH = 12.5, (middle) pH = 6, and (top) pH = 4. Scan rates are 150, 80 and 100 mV/s, respectively, but each surface is a new surface and therefore the quantity of material varies from one plot to the next. Each division on the y axis corresponds to 10 μA. The horizontal lines through each voltammogram are the zero current axes for the respective voltammogram. All scans here and in later figures were initiated from positive toward negative potentials and are shown with the cathodic (reduction) current at the bottom. They are all equilibrium scans.

have their current linearly dependent on scan rate indicative of a surface rather than diffusion process.

The zinc species is the easiest to understand, and its analysis provides useful data for interpreting the iron and cobalt data. Thus, Figure 4 shows data for zinc species **2** deposited on HOPG at low and high pH. In the range studied, one observes only one redox couple whose $E_{1/2}$ (average of anodic and cathodic peak) potential depends upon pH (Table III). The anodic and cathodic peak potentials are within 100 mV of each other at all pH values studied but with the greatest disparity occurring in strong base (Table III). In this sense the couple is reasonably reversible. The anodic and cathodic peak components do depend slightly on scan rate with their separation increasing with increasing scan rate (as is also observed in the iron and cobalt species voltammograms). This couple can only be assigned to the ring $Zn[Cl_{16}Pc(-2)]/Zn[Cl_{16}Pc(-3)]^-$ reduction process. The charge under the reduction peak is about 4 μC. Assuming the graphite surface is flat, and that the phthalocyanine molecules occupy an area of about 2×10^{-14} cm^2, this corresponds to a monolayer of dimeric aggregates.

In Table IV we compare the potentials for a range of phthalocyanine species both in solution and adsorbed on a graphite surface. Two general observations may be made:

(a) The ring Pc(−2)/Pc(−3) reduction process occurs at similar potentials in DCB solution and on an HOPG surface, *when this is immersed in aqueous base solution.*

(b) Electron acceptor substituents will shift the reduction couple to more positive potentials, while electron donor substituents will shift it to more negative potentials. For example, note the DMF solution data for zinc phthalocyanines in Table IV where octacyano substitution shifts this potential 760 mV positive of the unsubstituted ZnPc potential, while octabutoxy substitution shifts it 200 mV more negative.

Following observations a and b, with use of the datum for $Zn[Cl_{16}Pc(-2)]$/HOPG immersed in aqueous base at pH 10–13, the reduction process shifts positively in the sequence TNPc = OBuPc < Pc < $[Cl_{16}Pc(-2)]$ ≪ OCNPc. Thus, perchlorination makes the phthalocyanine ring a better acceptor but not to a dramatic degree.

The iron species **1**, adsorbed on HOPG, shows a well-behaved couple positive of zero whose identity, on the basis of previous iron studies,[44] is ascribed to $Fe^{III}[Cl_{16}Pc(-2)]^+/Fe^{II}[Cl_{16}Pc(-2)]$ (Figure 5). The anodic and cathodic peak potentials do not differ significantly from each other throughout the pH range (Table III). At any given pH its potential is more positive than for FePc or FeTsPc (Table IV) also indicative of the acceptor nature of the chlorine substituents. The corresponding $Co^{III}[Cl_{16}Pc(-2)]^+/Co^{II}[Cl_{16}Pc(-2)]$ couple is expected at very positive potentials in the voltammogram of species **3**, on the basis of previous experience,[44] and was not observed in the surface electrochemistry.

Both iron **1** (Figure 5) and cobalt **3** species (Figures 6 and 7) show a well-defined reduction wave whose potential is pH dependent throughout the pH range studied (1–14) (Figure 8) (Table

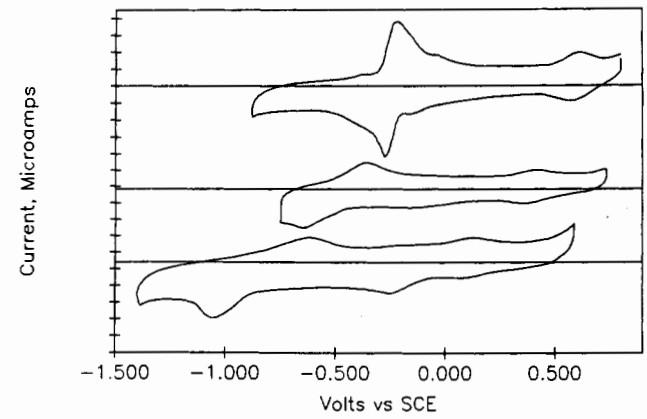

Figure 5. Surface electrochemical cyclic voltammograms for iron species **1** under argon at (bottom) pH = 11, (middle) pH = 5.7, and (top) pH = 2. Scan rates are 100, 200, and 100 mV/s, respectively. The y axis divisions are 10 μA. For other notes, see Figure 4. Also see Figure 9 for further iron data.

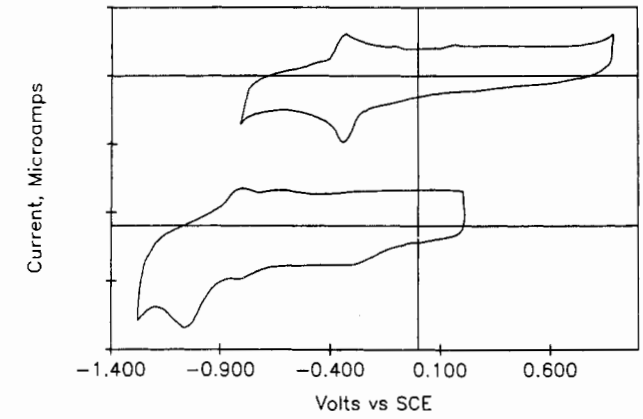

Figure 6. Surface electrochemical cyclic voltammograms for cobalt species **3** under argon at (bottom) pH = 10 and (top) pH = 2. The scan rate is 100 mV/s, and the y axis scale divisions are 10 μA. For other notes, see Figure 4.

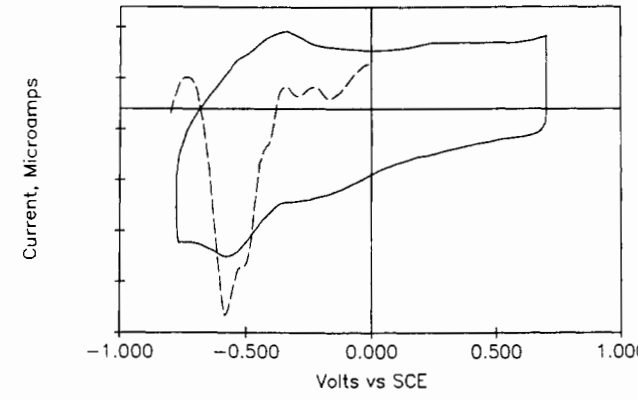

Figure 7. Surface electrochemical cyclic voltammogram for cobalt species **3** under argon at pH = 4, scan rate 100 mV/s. The y axis divisions are 5 μA. Superimposed is the surface electrochemical differential-pulse voltammogram for cobalt species **3** at a scan rate of 1 mV/s and pulse amplitude of 5 mV. The y axis divisions are each 1 μA for this plot. The plot is inverted from the more normal presentation to show reduction downward.

Both iron **1** (Figure 5) and cobalt **3** species (Figures 6 and 7) show a well-defined reduction wave whose potential is pH dependent throughout the pH range studied (1–14) (Figure 8) (Table

(44) Zecevic, Z.; Simic-Glavaski, B.; Yeager, E.; Lever, A. B. P.; Minor, P. C. *J. Electroanal. Chem. Interfacial Electrochem.* **1985**, *196*, 339–358.

Table III. Collection of Surface Electrochemical Data (V) versus pH for $M[Cl_{16}Pc(-2)]/[MCl_{16}Pc(-3)]^-$

pH	E_{pc}[a]	E_{pa}[b]	$E_{1/2}$[c]	$E(Fe^{II/I})$[d]	$E_{red}(O_2)$[e]	$E(Fe^{III/II})$[f]
			Iron Data (**1**)			
1.9	−0.23	−0.20	−0.22	−0.10 (0.01)		0.63 (0.08)
2.0	−0.24	−0.22	−0.23	−0.10 (0.12)	−0.14	0.60 (0.05)
2.6	−0.30	−0.24	−0.27			0.58 (0.08)
2.6	−0.30	−0.24	−0.27			0.58 (0.08)*[g]
3.0	−0.33	−0.29	−0.31		−0.265	
3.1	−0.36	−0.30	−0.33	−0.14 (0.12)		0.52 (0.06)
3.7	−0.40	−0.25	−0.32			0.53 (0.06)*
3.8	−0.39	−0.31	−0.35	−0.19 (0.13)		0.50 (0.07)
4.0	−0.43	−0.33	−0.38		−0.29	0.47
4.7	−0.53	−0.32	−0.42			0.43 (0.06)
5.0	−0.53	−0.37	−0.45		−0.34	
5.6	−0.56	−0.36	−0.46			0.42 (0.075)*
5.7	−0.64	−0.34	−0.49			0.40 (0.04)
6.0	−0.60	−0.36	−0.48		−0.30	
7.0	−0.65	−0.42	−0.53	−0.14	−0.27	0.34 (0.08)*
8.0	−0.77	−0.48	−0.62		−0.26	
8.6	−0.82	−0.44	−0.63			0.27 (0.04)*
8.8	−0.86	−0.48	−0.67	−0.17		0.24 (0.07)
9.0	−0.87	−0.50	−0.68		−0.29	
9.6	−0.86	−0.52	−0.69	−0.20 (0.2)		0.21 (0.08)
10.0					−0.27	0.22
11.0	−1.05	−0.61	−0.83		−0.28	
12.2				−0.25 (0)		−0.03 (0.05)
12.5	−1.12	−0.71	−0.91		−0.33	
13.0	−1.13	−0.76	−0.95	−0.25 (0)		−0.04 (0.03)*
			Zinc Data (**2**)			
2.5	−0.22	−0.17	−0.20			
3.5	−0.30	−0.25	−0.28			
4.0	−0.35	−0.25	−0.30			
6.0	−0.45	−0.40	−0.43			
8.0	−0.62	−0.41	−0.52			
10.0	−0.68	−0.60	−0.64			
12.5	−0.88	−0.75	−0.82			
			Cobalt Data (**3**)			
2.0	−0.33	−0.32	−0.33		−0.20	
3.0	−0.49	−0.31	−0.40		−0.27	
4.0	−0.53	−0.45	−0.49		−0.32	
5.0	−0.66	−0.42	−0.54		−0.39	
6.0	−0.68	−0.55	−0.62		−0.56	
7.0	−0.77	−0.61	−0.69		−0.51	
8.0	−0.85	−0.63	−0.74		−0.54	
10.0	−1.08	−0.67	−0.88		−0.45	
12.0	−1.22	−0.85	−1.04		−0.47	

[a] Cathodic peak potential for Pc(−2)/Pc(−3) anion reduction process. All data vs SCE, using cyclic voltammetry. [b] Anodic peak potential for Pc(−2)/Pc(−3) anion reduction process. [c] Average electrode potential for Pc(−2)/Pc(−3) anion reduction process. [d] Proposed Fe(II)/Fe(I) couple; peak to peak separation in parenthesis. [e] Oxygen reduction potential from peak of cyclic voltammogram under an oxygen atmosphere. [f] Fe(III)/Fe(II) redox potential; peak to peak separation in parenthesis. [g] All data were carried out on fresh surfaces except those with an asterisk, which were all collected on the same surface.

III). Both species show additional weak, poorly resolved waves on the positive side of the reduction wave (vide infra).

The strong reduction wave can be ascribed to one of three plausible processes, $M^{II}[Cl_{16}Pc(-2)]/M^{I}[Cl_{16}Pc(-2)]^-$, $M^{II}[Cl_{16}Pc(-2)]/M^{II}[Cl_{16}Pc(-3)]^-$, and $M^{I}[Cl_{16}Pc(-2)]^-/M^{I}[Cl_{16}Pc(-3)]^{2-}$, where this last possibility must assume that the $M^{II}[Cl_{16}Pc(-2)]/M^{I}[Cl_{16}Pc(-2)]^-$ is accounted for by the weaker poorly resolved structure positive of the main reduction wave.

Spectroelectrochemistry in solution (above) shows that reduction to $M^{I}[Cl_{16}Pc(-2)]^-$ occurs above −0.8 V in DMF, but this datum does not necessarily provide rigorous information for the adsorbed species.

In a determination of the nature of this reduction wave, certain observations can be made:

(c) Previous pH dependence studies of the $M^{II}Pc(-2)/[M^{I}Pc(-2)]^-$ process show that the potential is dependent upon pH in the acidic range but independent of pH in the basic range.[44-48]

Table IV. Variation of Redox Potentials (V) of Metal Phthalocyanine Redox Processes as a Function of Environment[a]

compd[b]	conditions[c]	$[MPc(-2)]/[MPc(-3)]^-$[d]	$[Co^{II}Pc(-2)]/[Co^{I}Pc(-2)]^-$	ref
		Cobalt		
CoTsPc/ads	aq pH 13	−1.37	−0.51	44
CoTsPc/ads	aq pH 2	−0.60	−0.31	44
CoTcPc/ads	1 M H_2SO_4	−0.42	−0.27	61
CoTNPc/ads	aq pH 8		−0.71	tw
CoTNPc/ads	aq pH 4		−0.57	tw
CoTNPc	DCB[e]	−1.56	−0.40	23
CoCRPc/ads	aq pH 11		−0.60	62
CoCRPc/ads	aq pH 2	−0.48	−0.34	62
CoPc	py		−0.61	63
CoPc/ads	aq pH 14		−0.57	64
CoPc/ads	aq pH 2		−0.29	64
		Zinc		
ZnTNPc	DCB[e]	−1.15		22
ZnTNPc/ads	aq pH 2	−0.48, −0.70		tw
ZnTNPc/ads	aq pH 10	−1.13		tw
ZnPc	DMF	−0.86		38
ZnOBuPc	DMF	−1.06		38
ZnOCNPc	DMF	−0.15		38

compd[b]		$[Fe^{I}Pc(-2)]^-/[Fe^{I}Pc(-3)]^{2-}$	Fe(II)/Fe(I)	Fe(III)/Fe(II)	ref
		Iron			
FeTsPc/ads	aq pH 10.7	−1.17	−0.51	0.02	56, tw
FeTsPc/ads	aq pH 3.5	−0.55	−0.30	0.42	56, tw
FePc/ads	aq pH 14		−0.68	−0.26	47, 48
FePc/ads	aq pH 2			0.39	47, 48
FePc	DMA	−1.17	−0.55	0.38	32

[a] Versus SCE. tw = this work. [b] TsPc = tetrasulfonated phthalocyanine; TNPc = tetraneopentoxyphthalocyanine, CRPc = tetracrownphthalocyanine, OBuPc = octabutoxyphthalocyanine, and OCNPc = octacyanophthalocyanine. ads = adsorbed on HOPG or OPG. [c] DCB = *o*-dichlorobenzene, DMF = dimethylformamide, py = pyridine, and DMA = dimethylacetamide. [d] M = Co(I) for cobalt complexes, and M = Zn(II) for zinc complexes. [e] Referenced internally against ferrocenium/ferrocene couple assumed to lie at 0.51 V vs SCE.

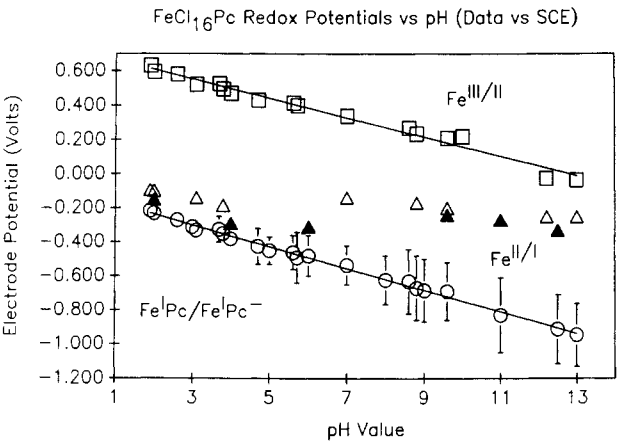

Figure 8. The pH dependences of the various surface waves using a modified iron species **1** HOPG electrode immersed in an appropriate phosphate buffer: $Fe^{III}[Cl_{16}Pc(-2)]^+/Fe^{II}[Cl_{16}Pc(-2)]$ couple, open squares; $Fe^{II}[Cl_{16}Pc(-2)]/Fe^{I}[Cl_{16}Pc(-2)]^-$ couple, closed triangles. For the $Fe^{I}[Cl_{16}Pc(-2)]^-/Fe^{I}[Cl_{16}Pc(-3)]^{2-}$ couple, the open circles show the average potentials, with the vertical bars indicating the anodic and cathodic component potentials. Their absence from a point means that the anodic–cathodic peak separation is less than 100 mV. The oxygen reduction potentials are indicated by open triangles. Note: The bars shown here are *not* error bars.

(d) Previous pH dependence studies of the $[M^{I}Pc(-2)]^-/[M^{I}Pc(-3)]^{2-}$ process show that the potential is dependent upon

(45) Elzing, A.; Van der Putten, A.; Visscher, W.; Barendrecht, E. *J. Electroanal. Chem. Interfacial Electrochem.* **1986**, *200*, 313.

pH through the entire pH range.[44]

(e) Previous studies of the $[M^{I}Pc(-2)]^{-}/[M^{I}Pc(-3)]^{2-}$ redox couple reveal that it is often much stronger and narrower than the $M^{II}Pc(-2)/[M^{I}Pc(-2)]^{-}$ redox process, especially in the alkaline regime.[44]

(f) The $M^{II}Pc(-2)/[M^{II}Pc(-3)]^{-}$ process has never been observed for MPc = CoPc or FePc. On the basis of the polarizing power of the central ion,[49] this couple would be expected to occur slightly positive of the corresponding zinc couple.

(g) The $M^{II}Pc(-2)/[M^{I}Pc(-2)]^{-}$ and $[M^{I}Pc(-2)]^{-}/[M^{I}Pc(-3)]^{2-}$ redox couples are within about 100–300 mV of each other in the acidic range, but their separation increases as pH increases above 7 because of their different pH dependence in this range.[44]

(h) The $Zn^{II}Pc(-2)/[Zn^{II}Pc(-3)]^{-}$ process occurs some 300–500 mV more positive than the $[M^{I}Pc(-2)]^{-}/[M^{I}Pc(-3)]^{2-}$ process (M = Co, Fe) in solution, depending upon substituent.[22,23] However, this difference is somewhat smaller when the species are in the adsorbed state.

(i) At any pH value, the first reduction wave of $Zn[Cl_{16}Pc(-2)]$ (**2**) occurs at a less negative potential than the primary reduction wave of either iron **1** or cobalt **3**.

(j) Perchlorinated phthalocyanine is a better acceptor ligand than Pc or TNPc. Not only will the $M^{III}[Cl_{16}Pc(-2)]^{+}/M^{II}[Cl_{16}Pc(-2)]$ (M = Co, Fe) wave be at a more positive potential than that for MPc, MTsPc, or MTNPc, but the $M^{II}[Cl_{16}Pc(-2)]/M^{I}[Cl_{16}Pc(-2)]^{-}$ and $M^{I}[Cl_{16}Pc(-2)]^{-}/M^{I}[Cl_{16}Pc(-3)]^{2-}$ waves should also lie at more positive potentials, for corresponding M.

Items c–j lead to only one tenable assignment for the reduction couple.

Thus, assignment to the $M^{II}[Cl_{16}Pc(-2)]/M^{II}[Cl_{16}Pc(-3)]^{-}$ process is excluded because observation f is incompatible with observation i. Assignment to the $M^{II}[Cl_{16}Pc(-2)]/M^{I}[Cl_{16}Pc(-2)]^{-}$ process is excluded because it could not be found so negative of the zinc couple in the basic range. If, energetically, such a process was very negative of the zinc couple, then reduction to $M^{II}[Cl_{16}Pc(-3)]^{-}$ would have to occur first, and this has already been excluded. Moreover, the pH dependence is not appropriate for this assignment.

However, assignment to the $M^{I}[Cl_{16}Pc(-2)]^{-}/M^{I}[Cl_{16}Pc(-3)]^{2-}$ process does not violate any of the observations noted above. Indeed such an assignment is specifically supported by the observed pH dependence, by the very narrow intense peak for this redox process, by the fact that it is observed negative of the corresponding zinc process at all pH values, and because of the fact that it occurs several hundred millivolts positive of the corresponding waves in the MPc and MTsPc species, at any given pH.

Both the iron and cobalt species, but not the zinc species, show a poorly resolved shoulder around 100 mV positive of the reduction wave in the acidic range. This is assigned to the $M^{II}[Cl_{16}Pc(-2)]/[M^{I}[Cl_{16}Pc(-2)]^{-}$ wave. In alkaline medium many of these species also show a more pronounced wave, positive of the reduction wave and close to or identical with the potential at which oxygen reduction occurs at the relevant pH value (Table III) (Figure 8). This might arise from the $M^{II}[Cl_{16}Pc(-2)]/[M^{I}[Cl_{16}Pc(-2)]^{-}$ process, but it may also be due to residual oxygen trapped in the electrode or leaking back slowly into the electrolyte despite the argon flow. This is demonstrated in Figure 9, where a small amount of oxygen has deliberately been admitted into the system, to delineate clearly the oxygen reduction potential in the presence of only trace oxygen.

Differential-pulse voltammetry has been carried out on the cobalt species **3** adsorbed on HOPG. A typical example is shown in Figure 7, where the modified HOPG electrode is immersed in buffer at pH 4. The broad cyclic voltammetric wave is clearly split into two components in the differential-pulse voltammogram. These may be the first two reduction processes, to $Co^{I}[Cl_{16}Pc(-2)]^{-}$ and then to $Co^{I}[Cl_{16}Pc(-3)]^{2-}$, but may also represent two different sites on the surface for the same reduction process.

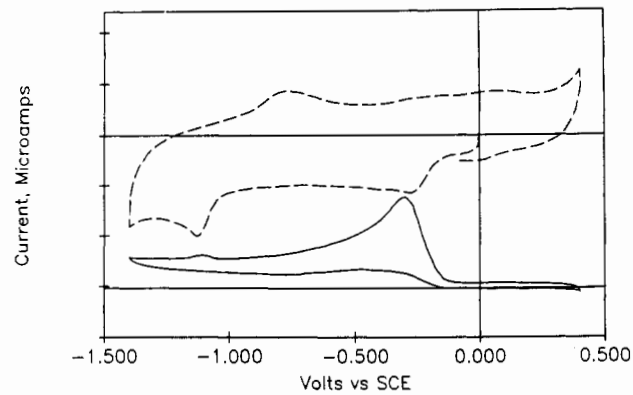

Figure 9. Surface electrochemical cyclic voltammograms for iron species **1** on an HOPG surface (top) under argon at pH = 14 (0.1 M KOH) (scan rate 100 mV/s, *y* axis scale divisions 5 μA apart) and (bottom) under an argon/oxygen mixture at pH = 14 (0.1 M KOH) (scan rate 100 mV/s, *y* axis scale divisions 50 μA apart). For the bottom voltammogram, only a dilute solution of oxygen in an aqueous KOH was added to demonstrate probable origin of the first negative reduction wave under argon.

Thus, the main reduction wave seen in all three complexes is the ligand anion radical wave of zinc(II), cobalt(I), and iron(I).

pH Dependence. Reduction Couple. All three species show a similar pH dependence; the iron species **1** was chosen for the most detailed analysis. Thus, the anodic and cathodic peak components shift to more negative potentials with increasing pH, throughout the entire pH range studied (1–14). The actual positions of the reduction peaks and their degree of structure are somewhat sensitive to variation in surface morphology from one surface to another. The separation between the peak potentials also tends to increase with increasing pH (see Table III and Figure 8). However, the average peak positions are reproducible (error ± 20 mV). The best lines are (data in volts for $M[Cl_{16}Pc(-2)]/M[Cl_{16}Pc(-3)]^{-}$):

iron (**1**)	$E = -0.064pH - 0.11$	$R = 0.997$ for 23 points
zinc (**2**)	$E = -0.060pH - 0.06$	$R = 0.998$ for 7 points
cobalt (**3**)	$E = -0.069pH - 0.20$	$R = 0.999$ for 9 points

The most reasonable explanation of the pH dependence follows from the fact that the potential in organic solvents is most similar to that in basic media. Under such circumstances the molecule being reduced in solution is essentially the same as that on the surface. However with decreasing pH, protonation occurs at the peripheral nitrogen atoms because the phthalocyanine is negatively charged for zinc and dinegatively charged for iron and cobalt.

The increasing separation between anodic and cathodic peak components at higher pH is much more pronounced for iron and cobalt than for zinc. Once the material is reduced, there is evidently some change in electronic structure such that the reduced material becomes more difficult to oxidize. Since this occurs to a greater degree with the dinegative species than with the mononegative reduced **2**, it may be a consequence of enhanced binding to the graphite surface by the iron and cobalt species in their dinegative reduced state.

The $Fe^{III}[Cl_{16}Pc(-2)]^{+}/Fe^{II}[Cl_{16}Pc(-2)]$ couple is dependent upon pH across the entire pH range studied (1–14). The equation of the line is for species **1** (data in volts)

$$E(Fe^{III}/Fe^{II}) = -0.056pH + 0.72$$

$$R = 0.990 \text{ for } 18 \text{ points}$$

This is a surprising result clearly induced by the perchlorination substitution. Previous studies of the Fe(III)/Fe(II) redox process in iron phthalocyanine species have shown that this couple is independent of pH in the acidic region but has an approximately −59 mV/pH dependence in the basic regime.[44]

(46) Van der Putten, A.; Elzing, A.; Visscher, W.; Barendrecht, E. *J. Electroanal. Chem. Interfacial Electrochem.* **1987**, *233*, 113.
(47) Van der Putten, A.; Elzing, A.; Visscher, W.; Barendrecht, E. *J. Electroanal. Chem. Interfacial Electrochem.* **1986**, *214*, 523.
(48) Van der Putten, A.; Elzing, A.; Visscher, W.; Barendrecht, E. *J. Electroanal. Chem. Interfacial Electrochem.* **1987**, *221*, 95.
(49) Lever, A. B. P.; Minor, P. C. *Inorg. Chem.* **1981**, *20*, 4015–17.

Table V. Solution Electrochemical Data for $M[Cl_{16}Pc]$ in DMF

M	electrolyte	$E_{1/2}$, V vs SCE	assgnt	method[a]
Fe[b]	$(TBA)PF_6$	0.73	$Fe^{III}[Cl_{16}MPc(-2)]^+/Fe^{II}[Cl_{16}Pc(-2)]$	DPV
		-1.11	$Fe^{I}[Cl_{16}Pc(-2)]^-/Fe^{I}[Cl_{16}Pc(-3)]^{2-}$	
		-1.73	$Fe^{I}[Cl_{16}Pc(-3)]^{2-}/Fe^{I}[Cl_{16}Pc(-4)]^{3-}$	
Co[b]	$(TBA)PF_6$	1.09	$Co^{III}[Cl_{16}Pc(-2)]^+/Co^{II}[Cl_{16}Pc(-2)]$	DPV
		-1.21	$Co^{I}[Cl_{16}Pc(-2)]^-/Co^{I}[Cl_{16}Pc(-3)]^{2-}$	
		-1.69	$Co^{I}[Cl_{16}Pc(-3)]^{2-}/Co^{I}[Cl_{16}Pc(-4)]^{3-}$	
Zn	$LiCl/(TBA)PF_6$	-0.5	$Zn[Cl_{16}Pc(-2)]/Zn[Cl_{16}Pc(-3)]^-$	CV
		-0.8	$Zn[Cl_{16}Pc(-3)]^-/Zn[Cl_{16}Pc(-4)]^{2-}$	

[a] DPV = differential-pulse voltammetry; CV = cyclic voltammetry. [b] These data were collected by using a AgCl/Ag electrode and referenced internally to the Fc^+/Fc couple assumed to lie at 0.40 V vs SCE in DMF. [c] $(TBA)PF_6$ = tetrabutylammonium hexafluorophosphate. Note that DPV peaks reported here do not correspond exactly with $E_{1/2}$ values.

The pH dependence in the alkaline regime is readily explained in terms of the binding of an OH^- group to $Fe^{III}[Cl_{16}Pc(-2)]^+$ and its absence from $Fe^{II}[Cl_{16}Pc(-2)]$ or perhaps, more likely, two OH^- groups bound to Fe(III) and one bound to Fe(II).

In the acidic range one might consider protonation of peripheral nitrogen atoms. However since this pH dependence is not observed in the unsubstituted FePc case, and since chlorination should reduce the basicity of these nitrogen atoms, such an explanation is not viable. Rather a water molecule may bind to $Fe^{III}[Cl_{16}Pc(-2)]^+$ and is rendered rather acidic by the acceptor nature of the chlorine substitution.

Solution Electrochemistry (Table V). Very dilute, apparently true solutions of $Zn[Cl_{16}Pc(-2)]$ (**2**) in $DMF/(TBA)PF_6$ show two reversible reduction waves separated by some 300 mV and evidently only to be associated with the two expected $Zn^{II}[Cl_{16}Pc(-2)]/Zn^{II}[Cl_{16}Pc(-3)]^-$ and $Zn^{II}[Cl_{16}Pc(-3)]^-/Zn^{II}[Cl_{16}Pc(-4)]^{2-}$ anion radical reduction processes.[22,50] The potential is similar to that of the surface under mild basic conditions (see a above). The voltammetry is consistent with the Nernst analysis of the data shown in Figure 3 and described above (but note different solvent system).

Oxidation waves near 0.6 and 1.0 V (vs SCE) observed for the iron **1** and cobalt **3** species when "dissolved" in $DMF/(TBA)PF_6$ are readily associated with the $M^{III}[Cl_{16}Pc(-2)]^+/M^{II}[Cl_{16}Pc(-2)]$ redox processes (M = Fe, Co). Scanning negatively therefrom, the first reduction waves are seen near -1.2 to -1.3 V for both species. These waves cannot be associated with the $M^{II}[Cl_{16}Pc(-2)]/[M^{I}[Cl_{16}Pc(-2)]^-$ redox process, since they are found significantly negative of those $M^{II}Pc(-2)/[M^{I}Pc(-2)]^-$ processes unequivocally identified in the voltammograms of CoTNPc and MTsPc (M = Co, Fe) (Table IV) (data for FeTNPc are not available). On the basis of the acceptor character of the chlorine substituents, such a process should be found positive of that observed in these latter species. The observed reduction waves are also considerably negative of the -0.8 V that the spectroelectrochemical studies showed to be more negative than the $M^{II}[Cl_{16}Pc(-2)]/[M^{I}[Cl_{16}Pc(-2)]^-$ couple.

However, these waves do occur at a position similar to that for the $M^{I}[Cl_{16}Pc(-2)]^-/M^{I}[Cl_{16}Pc(-3)]^{2-}$ surface wave when the modified electrode is immersed in strong alkaline medium. Thus, these solution reduction waves are assigned to $M^{I}[Cl_{16}Pc(-2)]^-/M^{I}[Cl_{16}Pc(-3)]^{2-}$ (M = Co, Fe). Evidently in parallel with the surface electrochemistry, the $M^{II}[Cl_{16}Pc(-2)]/[M^{I}[Cl_{16}Pc(-2)]^-$ couples for these perchlorinated phthalocyanines are broadened too much for observation, likely a consequence of aggregation and an associated slow kinetic pathway for electron transfer to the aggregate.

In a fashion similar to that of the zinc species **2**, both the cobalt and iron species show a second reduction process some 0.4–0.6 V more negative than the first. This may then be assigned to the $M^{I}[Cl_{16}Pc(-3)]^{2-}/M^{I}Cl_{16}Pc(-4)]^{3-}$ redox process, by analogy with previous solution observations.[22,50]

In conclusion the solution data do support the assignments made for the surface electrochemistry.

Electrocatalytic Oxygen Reduction. HOPG surfaces modified with **1** or **3** reduce oxygen electrocatalytically in a manner parallel to that observed with MPc,[50-55] CoTNPc,[15,16] and MTsPc (M = Co, Fe) species.[44,56,57] As shown in Figure 8, for species **1**, the peak potential for oxygen reduction is a function of pH only in acidic solutions where the slope of $E_p(O_2)$ vs pH is -(65–75) mV/pH unit. The cobalt species **3** reduces oxygen in the usual two-electron reduction to hydrogen peroxide and is also pH independent in the alkaline range (Table III). This conclusion arises from ring–disk experiments (not described in detail here) that show, at pH 10.1, hydrogen peroxide at the ring, formed concomitantly with oxygen reduction at the disk, when cobalt species **3** is the electrocatalyst.

The number of electrons involved in the iron **1** catalyzed reduction of oxygen is less certain due to poor reproducibility of current from one experiment to another (different surfaces). In alkaline medium, FePc is expected to be a four-electron reductant of oxygen to molecular oxygen (Figure 9). When iron species **1** is the electrocatalyst, at pH 10.1, in a ring–disk experiment, oxygen reduction occurring in the range 0 to -0.35 V (the peak of the cyclic voltammogram for oxygen reduction) (Figure 9) apparently produces water, there being no appreciable ring current. At potentials more negative than -0.35 V, oxygen reduction is associated with hydrogen peroxide detection at the ring. It seems secure that, like FePc, $Fe[Cl_{16}Pc(-2)]$ also acts as a four-electron catalyst in what is evidently a complex multipath oxygen reduction process.[45]

The low solubility of both the iron and cobalt species leads to some scatter in the oxygen reduction data. Since oxygen reduction at phthalocyanine-modified electrodes has been very extensively studied previously,[15,16,44,50-58] further discussion is not warranted here.

Note (Figure 9) that oxygen reduction occurs some 800 mV more positive than the principal reduction wave at pH 14. Previous studies[15] reveal that oxygen reduction generally occurs close to or slightly positive of the $M^{II}Pc(-2)/[M^{I}Pc(-2)]^-$ couple, and thus this observation provides further evidence that the principal reduction wave near -1.1 V (in Figure 9) cannot be the $M^{II}[Cl_{16}Pc(-2)]/[M^{I}[Cl_{16}Pc(-2)]^-$ reduction process.

Oxygen reduction, using **3**, occurs at a potential some 150–250 mV more positive than was observed with CoTNPc,[15] consistent with the stronger acceptor nature of the catalyst molecule. Previous studies have shown that the oxygen reduction potential tracks the pH dependence of the Co(II)/Co(I) couple.[15] Since

(50) Clack, D. W.; Hush, N. S.; Woolsey, I. S. *Inorg. Chim. Acta* **1976**, *19*, 129–32.
(51) Van Den Brink, F.; Visscher, W.; Barendrecht, E. *J. Electroanal. Chem. Interfacial Electrochem.* **1983**, *157*, 283–304.
(52) Van Veen, J. A. R.; Visser, C. *Electrochim. Acta* **1979**, *24*, 921–8.
(53) Van den Brink, F.; Barendrecht, E.; Visscher, W. *Recl. Trav. Chim. Pays Bas* **1980**, *99*, 253.
(54) Appleby, A. J.; Savy, M. *Electrochim. Acta* **1976**, *21*, 567–74.
(55) Appleby, A. J.; Fleisch, J.; Savy, M. *J. Catal.* **1976**, *44*, 281.
(56) Zagal, J.; Bindra, P.; Yeager, E. *J. Electroanal. Chem. Interfacial Electrochem.* **1980**, *127*, 1506.
(57) Zagal, J.; Sen, R. K.; Yeager, E. *J. Electroanal. Chem. Interfacial Electrochem.* **1977**, *83*, 207.
(58) Appleby, A. J.; Caro, P.; Savy, M. *J. Electroanal. Chem. Interfacial Electrochem.* **1980**, *111*, 91–6.
(59) Achar, B. N.; Fohlen, G. M.; Parker, J. A.; Keshavayya, J. *Polyhedron* **1987**, *6*, 1463–7.
(60) Freyer, W. *Z. Chem.* **1986**, *26*, 216–7.
(61) Kusuda, K.; Shiraki, K.; Yamaguchi, H. *Ber. Bunsen-Ges. Phys. Chem.* **1988**, *92*, 725–30.
(62) Kobayashi, N.; Lever, A. B. P. *J. Am. Chem. Soc.* **1987**, *109*, 7433–41.
(63) Lever, A. B. P.; Wilshire, J. P. *Can. J. Chem.* **1976**, *54*, 2514–6.
(64) Van Den Putten, A. Ph.D. Thesis, Amsterdam, 1986.

this oxygen reduction potential, in the acidic range, is about 100 mV positive of the main reduction wave, now assigned to $M^{I}[Cl_{16}Pc(-2)]^{-}/M^{I}[Cl_{16}Pc(-3)]^{2-}$, the inference is that the $M^{II}[Cl_{16}Pc(-2)]/[M^{I}[Cl_{16}Pc(-2)]^{-}$ couple is very close to and perhaps partially obscured by the main reduction processes. This adds support to the argument that the $M^{II}[Cl_{16}Pc(-2)]/[M^{I}[Cl_{16}Pc(-2)]^{-}$ process is represented by the shoulder on the positive potential side of the main reduction wave in acidic medium.

Conclusions

Perchlorination of the phthalocyanine ring leads to derivatives whose properties are clearly modified by the electron-withdrawing substituents. The species are much easier to reduce but more difficult to oxidize. The change in pH dependence for the $Fe^{III}[Cl_{16}Pc(-2)]^{+}/Fe^{II}[Cl_{16}Pc(-2)]$ couple relative to unsubstituted FePc reveals a new procedure for the tuning of a redox potential, in this case through a combination of pH control and ring substitution. In particular the central metal ion has gained additional Lewis acid character. The lack of clear observation of the $M^{II}[Cl_{16}Pc(-2)]/M^{I}[Cl_{16}Pc(-2)]^{-}$ redox process may arise through very sluggish kinetics, a consequence of the chlorine substitution generating aggregates, causing the wave to be broadened over an appreciable potential range. Further studies with other central metal ions are likely to prove rewarding.

Acknowledgment. We are indebted to the Natural Sciences and Research Council (Ottawa) and to the Office of Naval Research (Washington, DC) for financial support. We are indebted to Union Carbide, Parma, for a gift of highly oriented pyrolytic graphite.

Contribution from the Unité 219 de l'Institut National de la Santé et de la Recherche Médicale, Institut Curie, Section de Biologie, Centre Universitaire, 91405 Orsay, France

Influence of Distal Steric Hindrance on Multiple Energy Barriers in Ligand Binding to Heme Model Compounds

Catherine Tetreau,* Michel Momenteau, and Daniel Lavalette

Received June 19, 1989

The temperature dependence of carbon monoxide and oxygen binding to new "hybrid" heme model compounds has been investigated in liquid toluene between 180 and 320 K by laser flash photolysis. The heme models had been devised to present, on their distal face, a strong central steric hindrance. These compounds (except perhaps one) were found to react according to a double-barrier energy scheme, as already observed with basket-handle porphyrins. On moving along the reaction coordinate, the ligand must first overcome a free energy barrier due to the steric hindrance on the distal side. This external barrier and also the top of the internal energy barrier associated with bond formation are both increased in the more encumbered hemes. The ΔG changes are found to be nearly identical for CO and O_2, showing that steric discrimination against CO does not occur in the transition states. However, the relative contributions of enthalpy and entropy to the free energy changes associated with the innermost transition state differ sharply with the ligand.

Introduction

It is now generally recognized that binding of ligands to heme proteins is regulated by multiple free energy barriers.[1-3] Recently, we have reported that the reaction of oxygen and carbon monoxide with sterically protected heme model porphyrins, e.g. the basket-handle porphyrin **2**, (see Chart I), was similarly governed by two sequential barriers, whereas only one was found for a porphyrin devoid of any distal protection, e.g. compound **1**.[4] At a distance of 6-7 Å, the distal chain does not interfere with the Fe-O-O or Fe-C-O bond formation but produces a "matrix" effect, which is at the origin of the external barrier, by opposing the free diffusion of the ligand from the solvent. The innermost barrier remains characteristic of the ultimate bond formation process. These findings are consistent with a "peripheral" steric effect.[5,6] In an attempt to produce a strong "central" steric effect,[5,6] the "hybrid" models **3-5** have been recently synthesized.[7] Here, the pivalamido pickets are expected to maintain the "amide handle" approximately within a plane. However, since the possibility of anchoring an internal chelated proximal base is lost in **3-5**, an external nitrogenous ligand must be added to provide pentacoordination of the iron. Because of the distal steric hindrance, the base preferentially binds on the unprotected side of the porphyrin and leaves the encumbered distal cage for gaseous ligand binding. The most striking effect of increasing central steric hindrance from compound **3** to **5** is a reduction by a factor of 2500 of the affinity constant for CO while oxygen binding is reduced by less than a factor of 5 (at 293 K). Moreover, the changes affect mainly the "on" rate for CO while both "on" and "off" rates are changed in the case of oxygen.[7] Thus, constraining the handle in such a central position results in an increased sensitivity of rate and equilibrium constants upon changing the length of the distal chain.

The understanding of these effects, however, requires an investigation of the number and nature of the energy barriers. For this purpose, we investigate in this work the temperature dependence of the rate of CO and O_2 binding to 1-methylimidazole pentacoordinated porphyrins **3-5**.

Materials and Methods

The synthesis and characterization of porphyrins **3-5** as well as the procedures used for preparing the carboxy- and oxyhemochromes have been described previously.[7,8] Reduction to the Fe(II) forms was performed by using sodium dithionite in wet toluene under anaerobic conditions.[9] The pentacoordinated porphyrins were obtained by addition of a deaerated solution of 1-methylimidazole (1-MeIm). The solutions (about 5×10^{-5} M in toluene) were rendered anhydrous by prolonged bubbling with pure argon or CO. The final equilibration of the solutions

(1) Austin, R. H.; Beeson, K. W.; Eisenstein, L.; Frauenfelder, H.; Gunsalus, I. C. *Biochemistry* **1975**, *14*, 5355.
(2) Beece, D.; Eisenstein, L.; Frauenfelder, H.; Good, D.; Marden, M. C.; Reinisch, L.; Reynolds, A. H.; Sorensen, L. B.; Yue, K. T. *Biochemistry* **1980**, *19*, 5147.
(3) Ansari, A.; Di Iorio, E. E.; Dlott, D. D.; Frauenfelder, H.; Iben, I. E. T.; Langer, P.; Roder, H.; Sauke, T. B.; Shyamsunder, E. *Biochemistry* **1986**, *25*, 3139.
(4) Tetreau, C.; Lavalette, D.; Momenteau, M.; Lhoste, J. M. *Proc. Natl. Acad. Sci. U.S.A.* **1987**, *84*, 2267.
(5) Traylor, T. G.; Campbell, D.; Tsuchiya, S.; Mitchell, M.; Stynes, D. V. *J. Am. Chem. Soc.* **1980**, *102*, 5939.
(6) Hashimoto, T.; Dyer, R. L.; Crossley, M. J.; Baldwin, J. E.; Basolo, F. *J. Am. Chem. Soc.* **1982**, *104*, 2101.
(7) Momenteau, M.; Loock, B.; Tetreau, C.; Lavalette, D.; Croisy, A.; Schaeffer, C.; Huel, C.; Lhoste, J. M. *J. Chem. Soc., Perkin Trans. 2* **1987**, 249.
(8) Lavalette, D.; Tetreau, C.; Mispelter, J.; Momenteau, M.; Lhoste, J. M. *Eur. J. Biochem.* **1984**, *145*, 555.
(9) Momenteau, M. *Biochem. Biophys. Acta* **1973**, *304*, 814.

0020-1669/90/1329-1727$02.50/0